Environmental Science & Technology

Article

Cite This: Environ. Sci. Technol. XXXX, XXX, XXX−XXX

pubs.acs.org/est

The Cooling Rate- and Volatility-Dependent Glass-Forming Properties of Organic Aerosols Measured by Broadband Dielectric Spectroscopy

Yue Zhang,[*,†,‡,§] Leonid Nichman,[†,#] Peyton Spencer,[†] Jason I. Jung,[†] Andrew Lee,[†,⊥] Brian K. Heffernan,[†] Avram Gold,[§] Zhenfa Zhang,[§] Yuzhi Chen,[§] Manjula R. Canagaratna,[‡] John T. Jayne,[‡] Douglas R. Worsnop,[‡] Timothy B. Onasch,[†,‡] Jason D. Surratt,[§] David Chandler,[∥,▽] Paul Davidovits,[*,†] and Charles E. Kolb[*,‡]

[†]Department of Chemistry, Boston College, Chestnut Hill, Massachusetts 02459, United States

[‡]Aerodyne Research Inc., Billerica, Massachusetts 01821, United States

[§]Department of Environmental Sciences and Engineering, Gillings School of Global Public Health, University of North Carolina at Chapel Hill, Chapel Hill, North Carolina 27599, United States

[∥]Department of Chemistry, University of California, Berkeley, Berkeley, California 94720, United States

Supporting Information

ABSTRACT: Glass transitions of secondary organic aerosols (SOA) from liquid/semisolid to solid phase states have important implications for aerosol reactivity, growth, and cloud formation properties. In the present study, glass transition temperatures (T_g) of isoprene SOA components, including isoprene hydroxy hydroperoxide (ISOPOOH), isoprene-derived epoxydiols (IEPOX), 2-methyltetrols, and 2-methyltetrol sulfates, were measured at atmospherically relevant cooling rates (2−10 K/min) by thin film broadband dielectric spectroscopy. The results indicate that 2-methyltetrol sulfates have the highest glass transition temperature, while ISOPOOH has the lowest glass transition temperature. By varying the cooling rate of the same compound from 2 to 10 K/min, the T_g of these compounds increased by 4−5 K. This temperature difference leads to a height difference of 400−800 m in the atmosphere for the corresponding updraft induced cooling rates, assuming a hygroscopicity value (κ) of 0.1 and relative humidity less than 95%. The T_g of the organic compounds was found to be strongly correlated with volatility, and a semiempirical formula between glass transition temperatures and volatility was derived. The Gordon−Taylor equation was applied to calculate the effect of relative humidity (RH) and water content at five mixing ratios on the T_g of organic aerosols. The model shows that T_g could drop by 15−40 K as the RH changes from <5 to 90%, whereas the mixing ratio of water in the particle increases from 0 to 0.5. These results underscore the importance of chemical composition, updraft rates, and water content (RH) in determining the phase states and hygroscopic properties of organic particles.

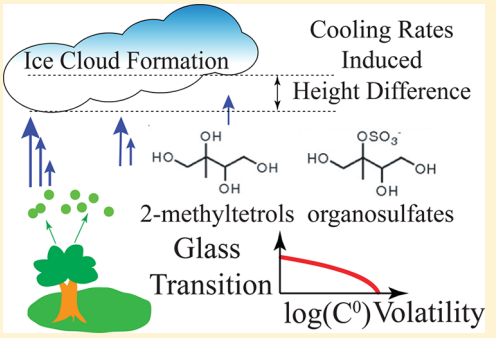

1. INTRODUCTION

Oxidized organic species comprise a large fraction (20−80%) of submicron atmospheric aerosol particulate matter (PM), especially outside large urban and intensive industrial regions.[1] Secondary organic aerosols (SOA) account for a large fraction of the organic particulate matter.[2] SOA is formed by gas phase oxidation products of volatile and semivolatile organic species that have condensed on pre-existing aerosol particles, undergone multiphase chemistry reactions, or nucleated with other secondary pollutants like sulfuric acid to form new particles.[3] It was initially assumed that organic aerosols (OA) would always be liquid, particularly at high relative humidity where organic and inorganic water-soluble PM components deliquesce.[4,5] However, recent evidence suggests that both laboratory-simulated and ambient atmospheric SOA particles are often solid (glassy) or semisolid in low-to-medium humidity environments and become liquid at relative high humidity.[6−14] For instance, inertial impaction studies have shown that a large fraction of SOA particles produced in Finnish forests as well as in environmental chambers and flow reactors from biogenic and anthropogenic organic precursor vapors bounce, indicating that they are in a solid or semisolid state.[14,15] It is clear that these solid or semisolid particles are not organic crystals, because they are created by photochemical processes known to produce a large number of distinct semivolatile products that co-condense, thereby inhibiting crystallization.[16] This study focuses on examining the effects of cooling rates, volatility, and

Received: June 3, 2019
Revised: August 19, 2019
Accepted: September 6, 2019
Published: September 6, 2019

Downloaded via UNIV OF NEW ENGLAND on October 22, 2019 at 06:37:05 (UTC).
See https://pubs.acs.org/sharingguidelines for options on how to legitimately share published articles.

© XXXX American Chemical Society

DOI: 10.1021/acs.est.9b03317
Environ. Sci. Technol. XXXX, XXX, XXX−XXX

water content on the glass transitions of organic compounds and its atmospheric implications. To investigate the above effects, the glass transition temperatures of SOA surrogates and isoprene-derived SOA components, which include isoprene hydroxy hydroperoxides (1,2-ISOPOOH), *trans*-β-isoprene epoxydiols (*trans*-β-IEPOX), 2-methyltetrols (2-MT), and 2-methyltetrol sulfates (2-MT-OS), were measured by broadband dielectric spectroscopy (BDS). The above isoprene-derived compounds represent different stages of the isoprene oxidation process in the atmosphere and thus have decreasing volatility, which makes them ideal for examining the effects of volatility on the glass transition temperature. ISOPOOH is the most volatile species of the four and is produced from the gas phase oxidation of isoprene by OH and HO_2 radicals.[17] Further reaction of ISOPOOH with OH radicals generate IEPOX, a semivolatile compound that can partition between particles and the gas phase.[18] Heterogeneous reactions of IEPOX with acidified sulfate particles produce semivolatile condensed phase species, including 2-methyltetrol, alkene triols, and organosulfates such as 2-methyltetrol sulfates.[19,20] 2-Methyltetrol and 2-methyltetrol sulfates can account for up to 30 and 65% of the isoprene-derived SOA mass from the flow tube and chamber studies, respectively.[21−25]

The glassy phase state of atmospheric organic compounds is important not only for understanding the science related to their evolution and reactivity but also for their influence on climate change and air quality[26−30] through effects on heterogeneous reactions with trace gases[31,32] as well as altering ice nucleation properties.[33−35] The increased ability of glassy OA to nucleate ice crystals that form cirrus clouds in the upper troposphere may be particularly important given the key role these clouds have in global warming.[26,36] There has been considerable progress in predicting the ice nucleation properties of organic aerosols in the past decade. Koop et al. have estimated glass transition temperature (T_g) values of 268−290 K for a range of surrogate biogenic SOA compounds, with oxidation and/or oligomerization reactions leading to higher molecular weight and/or more viscous products with higher T_g.[27] Dette et al. used the "metastable aerosol by low temperature evaporation of solvent (MARBLES)" techniques to measure the glass transition temperatures of binary mixtures of the oxidation products of α-pinene SOA as well as organic−inorganic mixtures.[37,38] Berkemeier et al. and Lienhard et al. examined the effects of relative humidity and water content on the glass transition of organic aerosols as well as how water diffusion is controlled by cooling rates and temperatures.[39,40] Their findings indicate that diffusivity of water can influence the glass transition process for organic aerosols, depending on the conditions.[39,40] Another factor that can directly influence the glass formation is the cooling rate. Previous studies have shown that a faster cooling rate enables the supercooled liquid molecules to fall out of equilibrium sooner and thus makes these molecules become glass at a higher temperature.[41,42] However, few studies have attempted to quantify either the influences of cooling rate on the glass transition temperatures or the implications of such effects in the ambient environment.[43] Experimental data on the glass transition of atmospherically relevant organic components, including the effects of cooling rates and water content on glass transitions of organic aerosols, are also limited.[27,44]

In a previous study, we have shown that broadband dielectric spectroscopy (BDS) of aerosol particles deposited in the form of a thin film onto an interdigitated electrode (IDE) provides dipole relaxation rates for organic aerosols as a function of temperature.[44] We have demonstrated that this IDE-BDS technique can be used to characterize glass transitions for both simulated and ambient organic aerosols. In the present study, we use this technique to address some of the currently less well understood aspects of liquid-to-glass phase transitions of atmospherically important organic aerosols. We conducted experiments that examined four topics: (i) the glass transition temperatures of isoprene hydroxy hydroperoxides (1,2-ISOPOOH), *trans*-β-isoprene epoxydiol (*trans*-β-IEPOX), 2-methyltetrol, and 2-methyltetrol sulfates, all compounds that are oxidation products of isoprene in the ambient environment and can form isoprene-derived SOA,[20,22,45] which were measured by thin film BDS; (ii) the dependence of glass transition on the cooling rate at atmospherically relevant cooling rates from 2 to 10 K/min which was measured to parameterize the effects of updraft velocity on glass transition temperatures; (iii) the relationship between glass transitions of organic aerosols and their saturation vapor pressure; and (iv) the effect of water and additional organic components on the glass transitions of organic components.

Studying these four aspects of the glass transition process of the organic aerosols helps bridge the gap between laboratory measurements and atmospheric models by parameterizing the existing data for atmospheric modeling.

2. MATERIALS AND METHODS

Isoprene hydroxy hydroperoxide (1,2-ISOPOOH), *trans*-β-isoprene epoxydiol (*trans*-β-IEPOX), 2-methyltetrol (2-MT), and 2-methyltetrol sulfates (2-MT-OS) were synthesized in-house by published procedures.[46,47] The purity of the all the compounds was 99.9% except for 2-methyltetrol sulfates, which has a purity of 50.4%. The balance for the 2-methyltetrol sulfates samples was inorganic sulfates (ammonium bisulfates and ammonium sulfates).[23,46]

The experimental setup is shown in Figure S1 and is similar to that previously described.[44] The setup provides for sample generation via homogeneous nucleation of pure sample or binary mixtures, thin film formation via electrostatic precipitation on the IDE with associated humidity control, and temperature conditioning of the chamber and BDS measurement.

2.1. Sample Preparation and Broadband Dielectric Spectroscopy. The samples were prepared by two approaches. In the first method, in order to mimic the small size of ambient aerosols, the synthesized isoprene-derived SOA components are heated and homogeneously nucleated to form submicron particles. These particles are then electrostatically deposited onto the IDE substrates, as described by Zhang et al.[44] Briefly, the sample material to be studied (~0.2 g) is placed in a round-bottom flask equipped with a water-cooled condenser and heated to 50−65 °C.[48] A flow of 2 L/min dry air through the condenser carried the aerosol particles for precipitation onto the IDE. An IDE (NIB003744, MS-01/60, NETZSCH Instrument North America) is used in this study as a substrate for measuring the dielectric constants of organic materials. The IDE consists of two thin electrodes that are interdigitated like entwined finger tips. A stream of aerosolized oxygenated organic liquid droplets to be studied is passed through a high-voltage corona discharge (−5000 V) and directed over the substrate held at +3000 V within the precipitator. The charged particles are electrostatically

DOI: 10.1021/acs.est.9b03317
Environ. Sci. Technol. XXXX, XXX, XXX−XXX

Table 1. Measured and Predicted Glass Transition Temperatures of Selected Compounds and Estimated Saturation Vapor Pressures

compound	formula	T_g (K) (measured)[a]	T_g (K)[b] (predicted)	saturation vapor pressure (atm)
glycerol	$C_3H_8O_3$	<189 K (2 K min^{-1})[44] 192 ± 2 K (5 K min^{-1})[44] 194 ± 2 K (10 K min^{-1})[44]	208.5	(2.2 ± 0.6) × 10^{-7}, predicted[65,66]
ISOPOOH	$C_5H_{10}O_3$	142 ± 3 K (5 K min^{-1})	221.8	(6.3 ± 4.1) × 10^{-6},[c] predicted[91]
IEPOX	$C_5H_{10}O_3$	163 ± 2 K (2 K min^{-1}) 166 ± 2 K (5 K min^{-1}) 168 ± 2 K (10 K min^{-1}) 169 ± 2 K (15 K min^{-1}) 169.7 ± 2 K (20 K min^{-1})	221.8	(3.4 ± 1.9) × 10^{-6},[d] predicted[92]
lactose	$C_{12}H_{22}O_{11}$	379 ± 11 K[93]	336.7	(4.5 ± 4.1) × 10^{-19}, predicted[94]
3-methyl-1,2,3-butanetricarboxylic acid (3-MBTCA)	$C_8H_{12}O_6$	305 ± 5 K[38]	285.6	(2.2 $\pm^{1.5}_{1.6}$) × 10^{-13}, measured[95]
2-methyltetrol	$C_5H_{12}O_4$	226 ± 3 K (2 K min^{-1}) 230 ± 2 K (5 K min^{-1}) 232 ± 3 K (10 K min^{-1})	243.5	(2.1 $\pm^{20}_{1.9}$) × 10^{-8}, predicted[96]
2-methyltetrol sulfate	$C_5H_{12}O_7S$	276 ± 15 K (5 K min^{-1})	>298[e]	(2.2 $\pm^{20}_{2}$) × 10^{-11}, predicted[96,97]
citric acid	$C_6H_8O_7$	289.6 $\pm^{10}_{5}$ K (5 K min^{-1})[38,44,98,99]	292.5	1.0 × 10^{-9}–8.6 × 10^{-14},[f] measured[68]
1,2,6-hexanetriol	$C_6H_{14}O_3$	192–206 K[44,51,100]	227.0	(2.1 ± 1.2) × 10^{-9}, predicted and measured[66]
cis-pinic acid	$C_9H_{14}O_4$	268 ± 5 K[27]	262	(4.3 ± 3.8) × 10^{-10}, measured[101]
cis-pinonic acid	$C_{10}H_{16}O_3$	265 ± 11 K[27]	249	(7.6 ± 5) × 10^{-10}, measured[101]
di-*n*-butyl phthalate	$C_{16}H_{22}O_4$	174–180 K[44,102]	290.3	(3.9 ± 0.1) × 10^{-8}, measured[103]
dioctyl phthalate	$C_{24}H_{38}O_4$	190–194 K[44,73]	322.8	(1.3 ± 0.1) × 10^{-10}, measured[103]

[a]Brackets indicate the cooling rate at which the glass transition was measured. [b]The predicted T_g was based on the modeling parametrization in DeRieux and Li et al.[76] [c]The original paper did not specify an error bar. The error bar is based on the model performance discussion in the original manuscript.[104] [d]The vapor pressure was calculated by using the EVAPORATION model. The error bar is based on the evaluation of the model.[92] [e]An estimation based on DeRieux and Li et al. was used assuming one sulfur atom is an oxygen atom, as the original model does not include any parametrization of sulfur-containing compounds. Because the sulfur atom is heavier than the oxygen atom, organosulfate compounds should have a higher glass transition temperature than the CHO compounds with the same formula. Therefore, this is a lower-bound. [f]The experimental measurement for citric acid spanned a wide range of values. The final result we used is based on the averaged measured values for the vapor pressure of citric acid, $9 \times 10^{-12 \pm 1.5}$ atm.

deposited onto the substrate, gradually merging to form a thin film. The film was shown to have a roughness of 1 nm, and the thickness was calculated to be 5–10 μm based on a previous work.[49] The film thickness needed to be more than the IDE spacing to obtain the best signal reading.[50] In the second sample preparation method, ~50–100 μL of the samples (including 2-MT-OS, binary organic–organic mixtures, and the organic–water mixtures) is transferred onto the IDE substrate from a micropipette to cover the electrodes with a relatively thin film.

The BDS instrument used in this study is manufactured by NETZSCH Inc. (model DEA 288). The working principles of the instrument have been discussed in previous studies.[44,50] Briefly, the instrument is flushed with dry nitrogen until the dew point sensor (Honeywell Inc., Model HIH-40000-001) shows a dew point of the outflow to be less than −70 °C. An oscillating electric field applied to the IDE electrodes is scanned from 10^{-1} Hz to 1 MHz in 30 s, and the impedance of the sample (Z_{sample}) is measured as a function of the applied frequency. The dielectric constant (ε) of the sample can be derived from Z_{sample} via Eqn. (S1). The glass transition temperature of a compound is determined by deriving the relaxation timescale, τ, from fitting the Havriliak–Negami equation[44,51] for the dielectric constant and plotting log τ versus $1/T$, as described in a previous publication.[44] The detailed procedure for determining τ is illustrated in the Supporting Information (Eqns. S2 and S3).

Glycerol (99%, Sigma-Aldrich, St. Louis, MO, USA) was used in our previous study as the calibration compound for measuring the dielectric constant (ε) using the same setup, and the results match reported literature values.[44] The results demonstrate that our measurements of glass transition temperatures match those previously published results for both glycerol and citric acid.[44]

2.2. Cooling Rate and Water Content Control. The cooling rate-dependent glass transition was measured for single and binary organic samples prepared either as dry compounds or mixed with water. The sample was placed on an IDE inside a temperature conditioning chamber. The chamber consists of a stainless steel cap and a surface temperature controlled by a liquid nitrogen cooler or a resistive heater. The chamber is flushed with dry nitrogen gas to reduce the relative humidity (RH) prior to temperature conditioning. The size of the sample was inspected before and after the experiments to verify that there was no significant evaporation or condensation of the water and organic compound. The small volume of the sampling chamber (~77 cm^3) is likely not going to alter the liquid content of the organic–water mixture significantly. The Gordon–Taylor equation (Eqn. S4) was used to calculate the glass transition temperature of organic–water mixtures, and these calculated T_g values were compared with the measured results. The sample temperature can be controlled between −150 and +200 °C. The typical cooling cycle starts at approximately 20 °C and ends at about −140 °C. The cooling

DOI: 10.1021/acs.est.9b03317
Environ. Sci. Technol. XXXX, XXX, XXX–XXX

cycles are adjusted to three desired cooling rates that are comparable to ambient atmospheric conditions: 2, 5, and 10 K/min. Details of the experimental setup are shown in Figure S1.

2.3. Calculation of Cooling Rate-Dependent Glass Transition Temperatures. The glass transition temperature is known to change with the sample cooling rate. Kinetic theories have shown that as a compound is cooled and transformed from liquid to supercooled liquid, the decrease in the thermal motion of molecules results in an increase in the timescale of molecules to reach equilibrium with any other perturbations, which is defined as the relaxation timescale. The logarithm of the relaxation timescale of the supercooled liquid molecules versus $1/T$ often exhibits a super-Arrhenius behavior.[43,52] As the temperature further decreases and the equilibrium rate exceeds the cooling rate, the liquid compound reaches the glassy state. The logarithm of relaxation timescale of the molecules versus $1/T$ then shows an Arrhenius behavior.[53] As the cooling rate increases, the temperature at which the liquid can no longer maintain thermal equilibrium also increases, corresponding to a higher glass transition temperature, as shown in Figure S2. This theory was incorporated into the "East Model" by Chandler et al. to predict glass-forming processes and has been shown to match experimental results.[28,42] Similarly, because the BDS instrument can provide the equilibrium relaxation timescale of the sample organic molecules, it can determine when a compound no longer maintains liquid equilibrium and becomes glass at the selected cooling rate.

3. RESULTS AND DISCUSSION

3.1. Glass Transition Temperature of SOA Compounds and Surrogates. Table 1 shows the glass transition temperature and saturation vapor pressure of selected organic compounds and isoprene-derived SOA components from this study and previous studies.[27,44,51] The volatilities of the compounds in Figure 1 decrease as the compounds become more highly functionalized with oxidation.

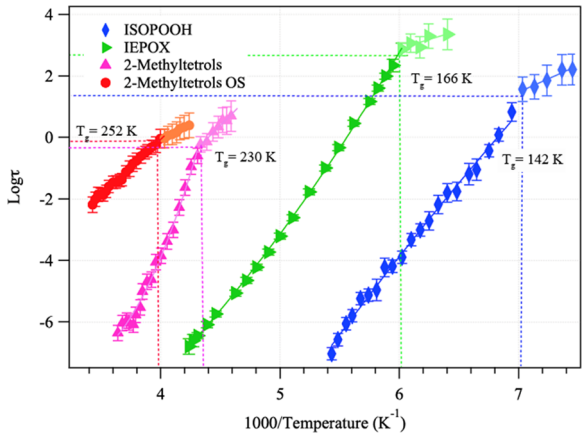

Figure 1. Logarithm of the relaxation timescale versus 1000/temperature (K^{-1}) of isoprene oxidation products at a 5 K/min cooling rate. The darker color shades represent the super-Arrhenius region, and the lighter color shades represent the Arrhenius region. The intersection between the Arrhenius and the super-Arrhenius curves determine the glass transition temperatures. A high-resolution plot of the glass transition of 2-methyltetrols and 2-methyltetrol sulfates can be seen in Figure S1.

The relaxation time, τ, of each sample compound as a function of BDS input frequency and temperature is shown in Figure 1.[44] Based on the East Model theory describing the glass transition processes, log τ values obtained at the higher temperature range are fitted to the super-Arrhenius function, and the data obtained at the lower temperature range are fitted to the Arrhenius function.[28,43,53,54] The intersection between the super-Arrhenius and the Arrhenius curves corresponds to the glass transition temperature.

Figure 2 shows the experimental values of glass transition temperatures of three sample compounds at a 5 K/min cooling rate obtained by the procedure described. The glass transition temperatures of ISOPOOH and IEPOX are 142 ± 3 and 166 ± 2 K, respectively, while 2-methyltetrol shows a much higher glass transition temperature of 230 ± 2 K. The glass transition temperature of 2-methyltetrol at a 10 K/min cooling rate is 232 K ± 3 K, which agrees within the error bar range of similar measurements performed by Lessmeier et al. using differential scanning calorimetry (DSC).[55] DSC uses faster cooling rates of 10−50 K/min, often leading to a difference of ∼10 K in T_g measurement when compared with the BDS method.[56] The 2-methyltetrol sulfates with inorganic sulfates mixture have a glass transition temperature of 252 ± 3 K. Each experiment was repeated at least three times to calculate the average relaxation time and the standard deviation at each temperature, as shown in Figure 2 and Figure S3. The error bars for the glass transition temperatures are calculated based on one standard deviation of the pre-averaged fitting curves in the super-Arrhenius and Arrhenius regions. The data points in the transitional region between the super-Arrhenius and the Arrhenius sections are fitted with both formulas and should belong to the fittings that generated the higher coefficients of determination (R^2). Murray et al. showed that the phase state of the organic aerosols could impact their ice nucleation

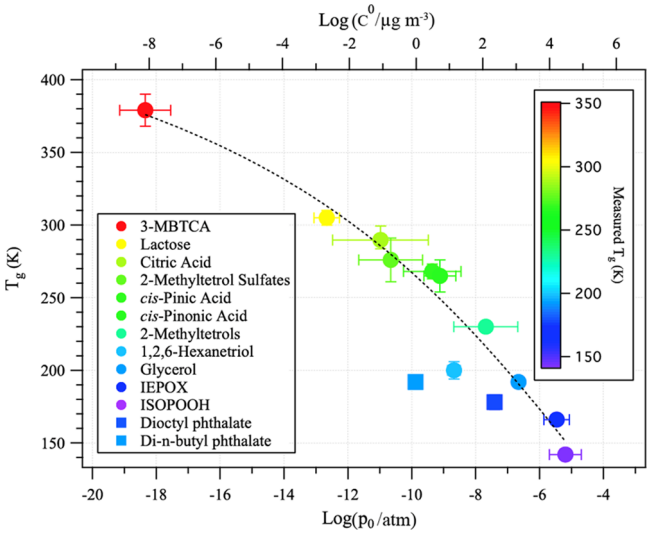

Figure 2. Glass transition temperatures (at 5 K/min cooling) of isoprene oxidation products and compounds from additional studies[44,65−68] as a function of the saturation vapor pressure (bottom x axis) and effective saturation concentration (top x axis, assuming an average molar mass of 200 g mol^{-1} and activity coefficient of 1). The colors and the error bars of the data points are based on the measured glass transition temperatures shown in Table 1. The dashed curve represents a fitted function for $\log(p_o)$ versus T_g of all compounds excluding aromatic components (phthalates).

DOI: 10.1021/acs.est.9b03317
Environ. Sci. Technol. XXXX, XXX, XXX−XXX

properties, with enhanced heterogeneous ice nucleation observed for aerosols in glassy phase states.[57] The T_g of pure 2-methyltetrol sulfates is determined to be 276 ± 15 K by applying the purity and glass transition temperatures of the mixture and inorganic sulfates (assuming all sulfates were ammonium bisulfate) to the Gordon−Taylor equation (Eqn. S4), with the details of the calculation shown in the Supporting Information. The higher glass transition temperature of 2-MT and 2-MT-OS indicates that isoprene-derived SOA, which contains a large mass ratio of 2-MT and 2-MT-OS, is likely able to reach the glassy phase state in the upper troposphere, where temperatures are often below −45 °C.[58] The relatively high glass transition temperatures of 2-methyltetrol and 2-methyltetrol sulfates make them candidates to nucleate ice heterogeneously and potentially promote the formation of cirrus clouds.[40,57]

The vapor pressure, glass transition temperature, melting temperature, and viscosity are all influenced by the van der Waals forces between the molecules. Stronger van der Waals forces often lead to lower vapor pressures and melting temperatures, with higher glass transition temperatures and viscosities.[59,60] Koop et al. showed that there is a linear empirical relationship between the glass transition temperatures of organic compounds, T_g, with their melting temperatures, T_m, which can be expressed as $T_g \propto T_m$.[27] Trouton showed that the correlation between the enthalpy of evaporation, ΔH_{vap} ($\Delta H_{vap} \propto -\log p_{vap}$ at a given temperature), and the enthalpy of fusion, ΔH_{fus} ($\Delta H_{fus} \propto T_m$),[61] exists in many species, suggesting that the vapor pressure of a compound can be linked to its glass transition temperature through its melting temperature.[62] Wang and Richert show that there is a positive correlation between the glass transition temperature (T_g) and the boiling temperature (T_b) for a variety of liquids ($T_g \propto T_b$).[63] Because the boiling temperature is directly related to the enthalpy of evaporation ($T_b \propto \Delta H_{vap}$), the above relationship can be translated as the T_g is positively correlated with the enthalpy of evaporation ($T_g \propto \Delta H_{vap}$) and negatively correlated with the logarithm of the vapor pressure ($T_g \propto -\log p_{vap}$).[63] Modeling results reported by Shiraiwa et al. also suggest there is a relationship between the volatilities of the organic species and their glass transition temperatures.[64] The literature studies above suggest a potential monotonic relationship between the logarithm of vapor pressures and glass transition temperatures of chemical species. Hence, the logarithm of the predicted saturation vapor pressures of the compounds (p_o, atm) and their glass transition temperatures (Kelvin) obtained from the data of this study and the other studies[44,65−68] are shown in Figure 2, which exhibits a highly negatively correlated relationship.[65−68] Strong van der Waals forces tend to distort such semiempirical relationships;[69,70] therefore, aromatic (phthalate) compounds were excluded from calculating the correlation between $\log(p_o)$ versus T_g. Table 1 and Figure 2 show that the plot of $\log(p_o)$ versus T_g of the nonaromatic compounds follows a negatively correlated semiempirical relationship expressed in eq 1 and shown as a dashed curve in Figure 2.

$$T_g/\mathrm{K} = 480.07 - \frac{54395}{(\log_{10}(p_o/\mathrm{atm}) - 1.7929)^2 + 116.49} \quad (1)$$

In atmospheric sciences, the effective saturation concentration, C^* ($\mu g\ m^{-3}$), is often used rather than the pure compound saturation mass concentration C^0 ($\mu g\ m^{-3}$), Pankow et al. and Donahue et al. show that the p_o and C^* can be linked by the following equation:[4,71,72]

$$C^* = \frac{M10^6\zeta p_o}{RT}\frac{\Sigma_k C_k^{PM}}{M_i \Sigma_k \frac{C_k^{PM}}{M_k}} \approx \frac{M10^6\zeta p_o}{RT} = \zeta C^0 \quad (2)$$

where M_i is the molar mass of the organic compound i, (g mol^{-1}), ζ is the activity coefficient on mole fraction basis (often $0.3 < \zeta < 3$), R is the ideal gas law constant ($R = 8.2 \times 10^{-5}$ m^3 atm mol^{-1} K^{-1}), and T is the temperature (K), $\Sigma_k C_k^{PM}$ is the sum of all k organic compounds in the particle phase, representing the total organic mass concentration ($\mu g\ m^{-3}$), M_k is molar mass of compound k, and $\Sigma_k \frac{C_k^{PM}}{M_k}$ is the total moles of organic compounds in the particle phase. If assuming the molar masses of all the compounds in the aerosol phase were the same or very similar, the first part of Eq. (2) can be simplified to derive the second part with approximation. Therefore the main difference between C^0 and C^* is that C^* includes the effects of thermodynamic mixing and activity coefficient ζ that typically exist in complex mixtures.

By combining eqs 1 and 2, we also provide the correlation between the effective saturation concentration with the glass transition temperature in the following equation:

$$\begin{aligned} T_g &= 480.07 - \frac{54395}{\left(\log_{10}\left(\frac{RT}{M10^6}C^0\right) - 1.7929\right)^2 + 116.49} \\ &= 480.07 - \frac{54395}{\left(\log_{10}\left(\frac{RT}{M}C^0\right) - 7.7929\right)^2 + 116.49} \\ &= 480.07 - \frac{54395}{\left(\log_{10}\left(\frac{RT}{\zeta M}C^*\right) - 7.7929\right)^2 + 116.49} \end{aligned} \quad (3)$$

Equation 3 shows that the glass transition of the aerosol component is highly dependent on the pure compound saturation mass concentration C^0. Further, the glass transition temperature can be derived from the effective saturation concentration (C^*) or the volatility of SOA when the matrix effects between different organic components in the SOA are not strong. If assuming that the Gordon−Taylor coefficient between each organic component is 1,[38] then the average glass transition of an organic aerosol can be derived from the linear combination of its volatility bins.

Figure 3 compares T_g of the compounds investigated in this study and other studies[44,51,73−76] derived from modeling and experiments. The modeling results generally predict glass transition temperatures within 20 K of measured values, except for ISOPOOH, IEPOX, and aromatic phthalate compounds, where the modeling results overpredict T_g by up to 50 K. The DeRieux and Li et al. model used a total of 300 compounds to empirically fit the glass transition temperatures under dry conditions based on the number of carbon, hydrogen, and oxygen atoms. Overall, the DeRieux and Li et al. model did a reasonably accurate calculation for the T_g of CHO species, as shown in Figure 3. Because phthalate compounds are known to have relatively low T_g despite their relatively large molecular mass,[27,40,44] such data involving aromatic phthalate compounds showed deviations between measurements and models and were excluded in the linearity calculation. For instance, the

DOI: 10.1021/acs.est.9b03317
Environ. Sci. Technol. XXXX, XXX, XXX−XXX

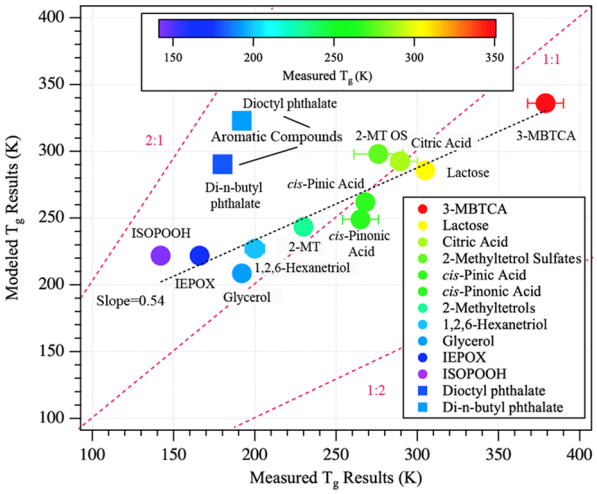

Figure 3. Comparison between the measured glass transition temperature from dielectric analysis and the modeled results based on DeRieux and Li et al.[76] The colors and the error bars of the data points are based on the measured glass transition temperatures shown in Table 1. The black dashed line represents the fitted line for all compounds excluding aromatic components (phthalates).

hydrperoxide group of ISOPOOH and epoxide group of IEPOX may also be able to explain the difference between the measured and the predicted values. Because the glass transition temperatures are known to be highly dependent on the molecular interactions and functional groups,[70,77,78] the model may not be able to accurately predict the glass transition temperatures of each individual compound, However, DeRieux and Li et al. model may still be useful for estimating the T_g of complex SOA mixtures as the averaged glass transition temperature of organic mixtures in the SOA system is likely going to follow the modeling result that is trained based on the statistical average of hundreds of compounds.

Studies also have shown that the molar mass of the organic compound could be an important variable in driving the T_g of dry organic components and an indication of the extent of intermolecular bonding.[11,15,27,79] Figure S4 shows the observed T_g of each compound in Table 1 as a function of its molar mass and oxidation state (oxygen-to-carbon ratio, O:C). A weak correlation was observed between the T_g and the inverse of the molar mass. The aromatic phthalate compounds also show a different trend compared with other CHO components in Figure S4, suggesting the importance of certain functional groups in altering the glass transition temperatures, which needs to be further examined. The relatively accurate prediction of glass transition temperatures using saturation vapor pressures in Figure 2 suggests that the vapor pressure of individual compounds and aerosol volatility may provide an alternative approach for easily estimating the glass transition temperatures of nonphthalate components by using eqs 1 and 3. The advantage of eq 1 is that it already considers the effects of molecular interactions on glass transition temperatures by incorporating the vapor pressure term. Equations 1 and 3 are based on the compounds investigated in this report; further studies on more organic compounds are needed in order to further improve the relationship of saturation vapor pressure and glass transition temperatures.

3.2. Effect of Cooling Rates on Glass Transition Temperatures. Experiments at three atmospherically relevant cooling rates were conducted to estimate the effects of the updraft rate of air parcels on the glass transition of SOA. The 2 K/min cooling rate is the baseline condition, indicating a relatively slow cooling rate of air parcels, while the 5 K/min cooling rate is a moderate cooling rate, and the 10 K/min cooling rate is a high-end estimate of the cooling rate that typically occurs in intense storm systems. The cooling rate-dependent glass transition temperatures of IEPOX and 2-methyltetrol are shown in Figure 4 and Figure S5: the glass

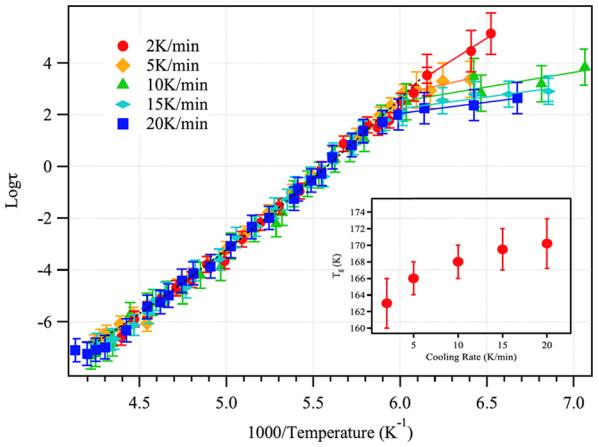

Figure 4. Logarithm of the relaxation time of IEPOX as a function of 1000/temperature (K^{-1}) with selected cooling rates. The inset shows the glass transition temperature derived from the relaxation times.

transition temperature increases by 5−6 K as the cooling rate changes from 2 to 10 K/min, and IEPOX shows a further increase of 2 K as the cooling rate changes from 10 to 20 K/min. The error bars in Figure 4 are estimated by calculating the slopes of the super-Arrhenius region and the Arrhenius region and where they intercept.[44] The 5 K change of glass transition temperature corresponds to 400−800 m of vertical height difference in the atmosphere, depending on the relative humidity of the environment and the hygroscopicity of the aerosol particles, assuming an environmental lapse rate of 6.49 K/km. The dependence of T_g on the cooling rate suggests that OA may become glassy at a lower altitude when the updraft rate of the air parcel is high. Besides the cooling rate-dependent glass transition temperatures measured in this study, a previous study also reported a similar difference of ∼5 K of T_g when the cooling rate increases from 2 to 10 K/min for other species, thus making the results above likely applicable to other organic aerosol systems as well.[80]

3.3. Effect of Organic Composition and Water Content on Glass Transition Temperatures. Atmospheric OA is composed of hundreds of molecular species having a wide range of functional groups and chemical composition.[81−83] Depending on the composition, these molecules can either have similar or distinct glass transition temperatures. Dette and Koop measured the glass transition temperatures of mixed SOA components having differences in T_g larger than 40 K.[37] However, the effects of mixtures and mixing ratios of SOA surrogates with similar glass transition temperatures are not well understood yet, as a previous work by Koop et al. reported that the Gordon−Taylor equation may not always work.[27] This study examines the glass transition temperatures of binary organic mixtures having similar T_g values as a function of mixing ratio. The difference in the glass transition temperature of the pure components in the mixtures ranges from 2 to 5 K.

DOI: 10.1021/acs.est.9b03317
Environ. Sci. Technol. XXXX, XXX, XXX−XXX

Figure 5 and Figure S6 show the measured glass transitions for binary mixtures of glycerol with 1,2,6-hexanetriol and glycerol with 1,4-butanediol, with the Gordon–Taylor constant (k_{GT}) being 0.798 and 0.802, respectively. In contrast to binary mixtures with >20 K difference in glass transition temperatures, the glass transition temperatures of binary mixtures with similar T_g do not follow the Gordon–Taylor equation, as similar deviations from the equation were also shown in other studies.[56,84−86]

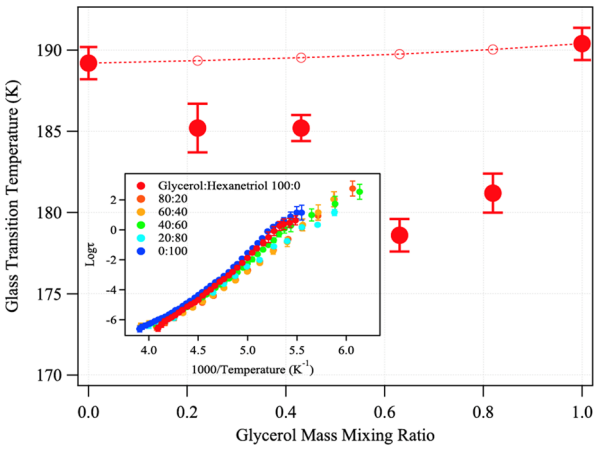

Figure 5. Glass transition temperatures of well-mixed binary glycerol/1,2,6-hexantriol solutions as a function of mixing ratio at the 5 K/min cooling rate. The results do not follow the Gordon–Taylor equation (dashed line). The insert shows the log τ of the mixture as a function of inverse temperature.

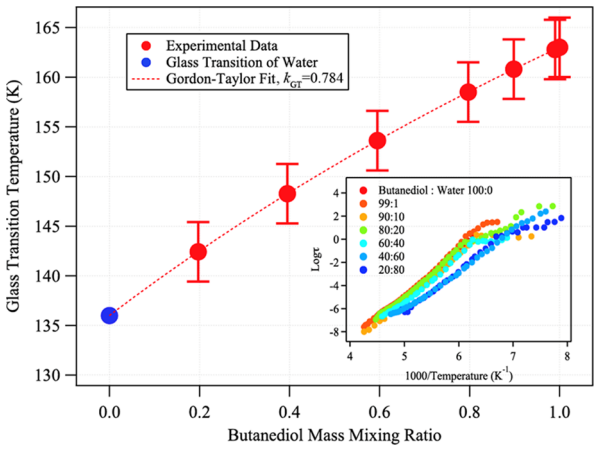

Figure 6. Glass transition temperatures of well-mixed aqueous 1,4-butanediol as a function of mixing ratio. The glass transition of water is 136 K.[105] The glass transition temperatures of the mixtures follow the Gordon–Taylor equation (dashed line). The inset shows the log τ of the mixture as a function of inverse temperature.

One theory proposes that the Gordon–Taylor nonlinear behaviors between mixtures were due to the increase or decrease in the entropy when the species were mixed together, which can be explained by the difference of the van der Waals forces and molecular interactions between different molecules.[87] The nonlinearity of the glass transition temperature of the two-component mixtures with similar T_g as shown here is likely due to the van der Waals forces between the two species, especially the additional hydrogen bonding formed between the two alcohol compounds in this study. Combining the results obtained from this study with those of Koop et al.[27] suggests that the glass transition of SOA may be heavily influenced by compounds that have large differences in T_g as well as those that have the largest mass fractions. Therefore, to estimate the glass transition temperature of SOA mixtures, the individual components comprising a mixture can be categorized into bins with a selected T_g range (e.g., 15 K bin width). The glass transition temperature within each bin does not follow the Gordon–Taylor equation because of the van der Waals force,[87,88] while T_g between different bins can be combined using the Gordon–Taylor equation.

Another important factor affecting the glass transition temperature of ambient OA is the water fraction within the particles. Ambient relative humidity levels can cycle from less than 20 to 100%, thereby altering the water content of OA particles and their glass transition temperatures. Water is known to reduce the glass transition temperature of OA by acting as a plasticizer; however, experimental data on the extent of this effect is limited. In this study, the effects of water content on the glass transition temperature of organic compounds are studied systematically by varying the mixing ratios of water and surrogate SOA compounds. Figure 6 shows the T_g of 1,4-butanediol–water mixtures as a function of mixing ratio, with k_{GT} = 0.784. A fit of the glass transition temperatures of the butanediol–water mixture is obtained by applying the Gordon–Taylor equation to the experimental data, assigning the T_g of pure water as 136 K. The fit to the data suggests that the Gordon–Taylor equation is applicable to such mixtures, possibly due to a relatively large difference in the glass transition temperatures of the organic compound and water. Using the 1,4-butanediol Gordon–Taylor factor as a surrogate for SOA, especially those containing multiple hydroxyl groups (such as isoprene-derived SOA), the effects of water content on the glass transition temperature of SOA can be estimated by applying Eqns. S4 and S7. The result is shown in Figure 7 when using a cooling rate of 2 K/min as the reference point of the T_g. Assuming ambient SOA have a density of 1.2 g cm^{-3} and a hygroscopicity factor κ of 0.1,[6] the relative humidity could reduce the glass transition temperatures by 10–40 K, depending on the humidity. At low-to-medium relative humidity (RH < 60%), both the cooling rate and water content have important effects on the glass transition temperatures of SOA, as a faster cooling rate and less water within the particles leads to an increase in the glass transition temperature. At high relative humidity (60% < RH < 90%), water plays a dominant role on the glass transition temperatures of SOA, which reduces T_g as much as 40 K for aerosols when compared with a dry environment.

3.4. Atmospheric Implications. The experimental data from this study indicate that by utilizing authentic standards from isoprene-derived SOA, aerosols containing a large fraction of these isoprene-derived compounds may have high enough glass transition temperatures that can lead to the transition from the liquid/semisolid state to glassy state in the upper troposphere. The transition to the glassy state reduces the oxidative reactivity of OA by OH radicals and ozone and also enhances deposition ice nucleation properties of aerosols. The glassy phase state also slows down the diffusion of gas phase molecules into the particles significantly, thereby limiting heterogeneous reactions and further aging of the aerosol particles.[89] Recent studies by Riva et al. and Cui et al. show

DOI: 10.1021/acs.est.9b03317
Environ. Sci. Technol. XXXX, XXX, XXX−XXX

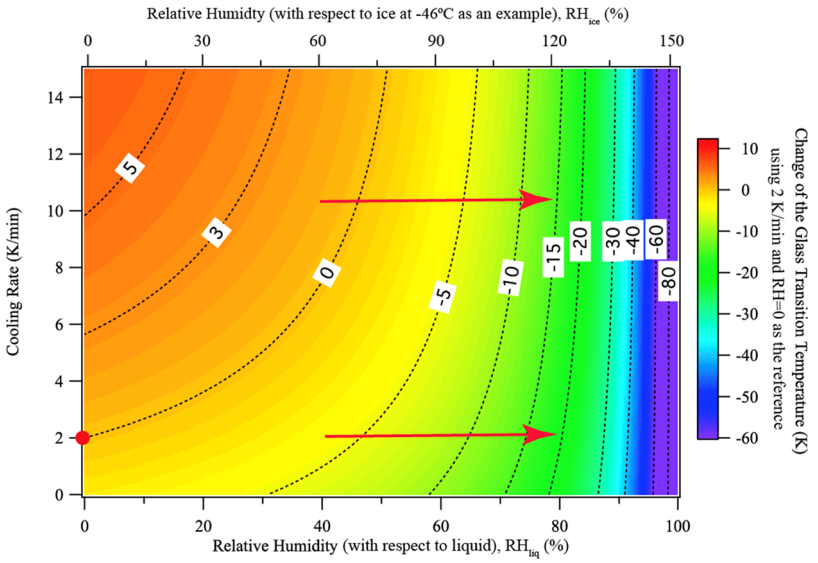

Figure 7. Effect of the cooling rate and water content on the glass transition temperatures of a SOA−water mixture, when using the 2 K/min cooling rate and zero water content (RH = 0) as a reference point shown as the red dot. The numbers show the decreased glass transition temperatures of the mixture when compared with the same mixture at the 2 K/min cooling rate and zero water content, which is indicated as the red dot. The hygroscopic coefficient, κ, is assumed to be 0.1. The bottom axis of the plot shows the relative humidity with respect to liquid water (RH_{liq}), while the top axis represents the relative humidity with respect to ice (RH_{ice}) at −46 °C as an example, where heterogeneous ice nucleation sometimes happens. The red solid arrows represent the relative humidity trajectories of aerosols with two different cooling rates, indicating that both cooling rates and water content influence the glass transition temperatures.

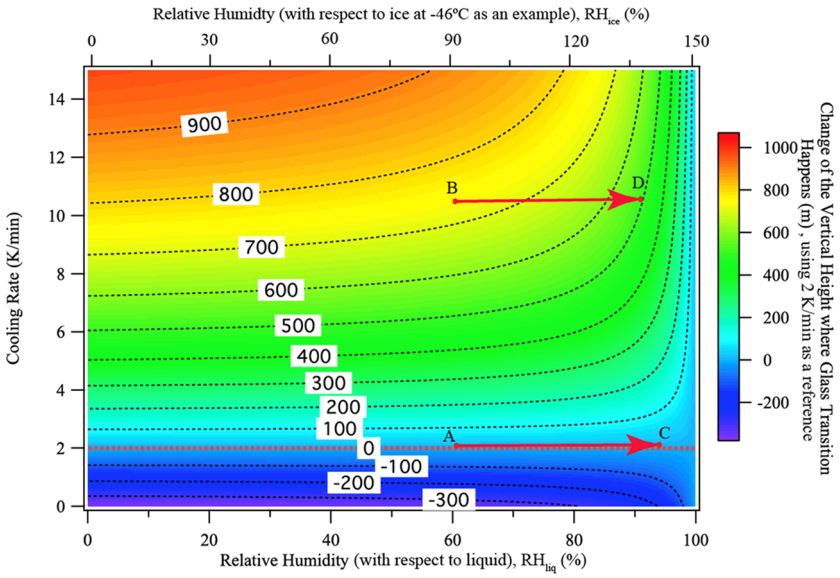

Figure 8. Effect of cooling rate on the glass transition temperatures of a SOA−organic mixture. The numbers show that the altitude difference (m) at which the SOA become glass referred to the same SOA at the 2 K/min cooling rate and respective water content, which is indicated in the plot as the red dotted line. A positive value means that the glass transition happens at a height lower than the reference 2 K/min cooling rate. The hygroscopic coefficient, κ, is assumed to be 0.1. The bottom axis of the plot shows the relative humidity with respect to liquid water (RH_{liq}), while the top axis represents the relative humidity with respect to ice (RH_{ice}) at −46 °C as an example, where heterogeneous ice nucleation sometimes happens. The red arrows represent the trajectories of aerosols with two different cooling rates, indicating that cooling rates have a relatively important effect on the height at which SOA become glass. The points in the figure represent four different RH and cooling rate conditions for the aerosols to become glass.

that, in isoprene-rich regions, such as the Southeastern United States or the Amazon rainforest, isoprene-derived organosulfates likely contribute to the relatively large fraction of the aerosol mass.[23,90] Shiraiwa et al. shows that the phase state of the aerosols depends on the ratio between the glass transition temperature and ambient temperature (T_g/T), with aerosols becoming glassy when $T_g/T \geq 1$.[64] Therefore, SOA are likely to form the glassy phase in the upper troposphere of these isoprene-rich regions where the temperature is well below the glass transition temperature of 2-MT-OS. Such transition of the phase state may reduce heterogeneous oxidation of aerosols in the upper troposphere and enhance ice cloud formation.[26] An improved understanding of the ice nucleation

DOI: 10.1021/acs.est.9b03317
Environ. Sci. Technol. XXXX, XXX, XXX−XXX

abilities of organic aerosols will help reduce the uncertainties of climate effects of aerosols.

It is worth noting that cooling rate and water content of the organic aerosols jointly impact the glass transition temperatures of OA in the atmosphere. The cooling rate, which can be correlated with the updraft rate of an air parcel, has been shown to influence the diffusion of water vapor, which alters the glass transition temperatures.[39,40] However, our study shows that cooling rates can also directly affect the altitude at which OA become glass, and the effects are more pronounced than its influence on the water diffusion to alter glass transition in the ambient environment. Water uptake due to RH changes can reduce the glass transition temperature by 20−30 K or more. By combining the experimental data on the water content and cooling rate on T_g, a model estimating the T_g of OA and the corresponding height differences were obtained to estimate the impact of the two atmospheric variables on the glass transition temperature, as shown in Figure 8 and Figure S8. A baseline of 2 K/min cooling with zero water content is applied to all scenarios for comparison. As shown in Figure 8, a cooling rate changing from 2 K/min (points A and C in the figure) to 10 K/min (points B and D in the figure) results in a height difference of up to 400−800 m for the glass transition, when the environmental RH is less than 90% and assuming a hygroscopic factor κ of 0.1.[76] The figure also shows that the initial environmental RH (especially when the RH is high) also has a significant effect on the height where particles become glass, when comparing the difference of height for points B and D. Figures S7 and S8 show the sensitivity analysis of the hygroscopicity on the glass transition temperatures. Based on the sensitivity analysis, the uncertainty of Figure 8 was determined to be ±100 m, indicating that the updraft rate of the aerosols can still have a significant impact on glass transitions of the organic aerosols. The difference of height when aerosols transform to the glassy state could also impact ice nucleation prediction as the current model does not consider the ice nucleation effects of organic aerosols and their phase state with height.

The findings of this research also suggest that the prediction of glass transition temperatures need to take the difference of T_g between different compounds into consideration. For compounds with T_g difference less than 5−10 K, the Gordon−Taylor equation may not be applicable. It is worth noting that the aerosol organic composition, water content, and cooling rate all need to be considered to predict the glass transition temperature of the particles over the range of ambient atmospheric conditions, which has profound implications on the reactivity and climate effects of OA.

■ ASSOCIATED CONTENT

Supporting Information

The Supporting Information is available free of charge on the ACS Publications website at DOI: 10.1021/acs.est.9b03317.

Working principles for broadband dielectric spectroscopy, the procedures to derive the relaxation times and the glass transition temperatures of the single organic compounds and mixtures, and detailed parametrization of the effects of water vapor and cooling rates on glass transition temperatures; Figure S1, the schematic diagram of the experimental setup; Figure S2, the procedures to derive the cooling rate-dependent glass transition temperatures; Figure S3, a high-resolution version for deriving the glass transition temperatures; Figure S4, the glass transition temperatures as a function of inverse molar masses and oxidation states; Figure S5, the cooling rate-dependent glass transition temperatures of 2-methyltetrol; Figure S6, the glass transition temperatures of binary mixtures of glycerol and 1,4-butanediols at selected ratios; Figure S7, the sensitivity analysis results of how the cooling rate and relative humidity affect the glass transition temperatures; Figure S8, the sensitivity analysis results of how the cooling rate and relative humidity influence the height where aerosols have glass transitions (PDF)

■ AUTHOR INFORMATION

Corresponding Authors

*E-mail: yzhang01@live.unc.edu. Phone: (978) 663-9500 ext. 301 (Y.Z.).
*E-mail: davidovi@bc.edu. Phone: (617) 552-3617 (P.D.).
*E-mail: kolb@aerodyne.com. Phone: (978) 663-9500 ext. 290 (C.E.K.).

ORCID

Yue Zhang: 0000-0001-7234-9672
Yuzhi Chen: 0000-0002-2547-8428
Timothy B. Onasch: 0000-0001-7796-7840
Jason D. Surratt: 0000-0002-6833-1450

Present Addresses

#Present address: National Research Council Canada, Flight Research Laboratory, Ottawa, Canada.
⊥Present address: Department of Chemistry, University of North Carolina, Chapel Hill, Chapel Hill, North Carolina 27599, Unites States.

Notes

The authors declare no competing financial interest.
∇Deceased April 2017.

■ ACKNOWLEDGMENTS

This material is based on work supported by the National Science Foundation (NSF) Environmental Chemistry Program in the Division of Chemistry under grant nos. 1506768, 1507673, and 1507642, and the National Science Foundation Division of Atmospheric and Geosciences grant no. 1524731. Y.Z. was supported by an NSF Postdoctoral Fellowship (AGS-1524731) and the National Institutes of Health (NIH) grant no. T32ES007018. We thank Shachi Katira, Juan P. Garrahan, Kranthi Mandadapu, Andrew T. Lambe, Daniel J. Czizco, Manabu Shiraiwa, Martin J. Wolf, Wen Xu, Eric Dong, and N. C. Armstrong for their kind support and assistance in the experiments and useful discussions.

■ REFERENCES

(1) Jimenez, J. L.; Canagaratna, M. R.; Donahue, N. M.; Prevot, A. S. H.; Zhang, Q.; Kroll, J. H.; DeCarlo, P. F.; Allan, J. D.; Coe, H.; Ng, N. L.; Aiken, A. C.; Docherty, K. S.; Ulbrich, I. M.; Grieshop, A. P.; Robinson, A. L.; Duplissy, J.; Smith, J. D.; Wilson, K. R.; Lanz, V. A.; Hueglin, C.; Sun, Y. L.; Tian, J.; Laaksonen, A.; Raatikainen, T.; Rautiainen, J.; Vaattovaara, P.; Ehn, M.; Kulmala, M.; Tomlinson, J. M.; Collins, D. R.; Cubison, M. J.; Dunlea, E. J.; Huffman, J. A.; Onasch, T. B.; Alfarra, M. R.; Williams, P. I.; Bower, K.; Kondo, Y.; Schneider, J.; Drewnick, F.; Borrmann, S.; Weimer, S.; Demerjian, K.; Salcedo, D.; Cottrell, L.; Griffin, R.; Takami, A.; Miyoshi, T.; Hatakeyama, S.; Shimono, A.; Sun, J. Y.; Zhang, Y. M.; Dzepina, K.; Kimmel, J. R.; Sueper, D.; Jayne, J. T.; Herndon, S. C.; Trimborn, A.

DOI: 10.1021/acs.est.9b03317
Environ. Sci. Technol. XXXX, XXX, XXX−XXX

M.; Williams, L. R.; Wood, E. C.; Middlebrook, A. M.; Kolb, C. E.; Baltensperger, U.; Worsnop, D. R. Evolution of organic aerosols in the atmosphere. *Science* **2009**, *326*, 1525−1529.
(2) Kroll, J. H.; Donahue, N. M.; Jimenez, J. L.; Kessler, S. H.; Canagaratna, M. R.; Wilson, K. R.; Altieri, K. E.; Mazzoleni, L. R.; Wozniak, A. S.; Bluhm, H.; Mysak, E. R.; Smith, J. D.; Kolb, C. E.; Worsnop, D. R. Carbon oxidation state as a metric for describing the chemistry of atmospheric organic aerosol. *Nat. Chem.* **2011**, *3*, 133−139.
(3) Schobesberger, S.; Junninen, H.; Bianchi, F.; Lönn, G.; Ehn, M.; Lehtipalo, K.; Dommen, J.; Ehrhart, S.; Ortega, I. K.; Franchin, A.; Nieminen, T.; Riccobono, F.; Hutterli, M.; Duplissy, J.; Almeida, J.; Amorim, A.; Breitenlechner, M.; Downard, A. J.; Dunne, E. M.; Flagan, R. C.; Kajos, M.; Keskinen, H.; Kirkby, J.; Kupc, A.; Kürten, A.; Kurtén, T.; Laaksonen, A.; Mathot, S.; Onnela, A.; Praplan, A. P.; Rondo, L.; Santos, F. D.; Schallhart, S.; Schnitzhofer, R.; Sipilä, M.; Tomé, A.; Tsagkogeorgas, G.; Vehkamäki, H.; Wimmer, D.; Baltensperger, U.; Carslaw, K. S.; Curtius, J.; Hansel, A.; Petäjä, T.; Kulmala, M.; Donahue, N. M.; Worsnop, D. R. Molecular understanding of atmospheric particle formation from sulfuric acid and large oxidized organic molecules. *Proc. Natl. Acad. Sci. U. S. A.* **2013**, *110*, 17223−17228.
(4) Donahue, N. M.; Robinson, A. L.; Stanier, C. O.; Pandis, S. N. Coupled partitioning, dilution, and chemical aging of semivolatile organics. *Environ. Sci. Technol.* **2006**, *40*, 2635−2643.
(5) Kamens, R.; Jang, M.; Chien, C.-J.; Leach, K. Aerosol Formation from the Reaction of α-Pinene and Ozone Using a Gas-Phase Kinetics-Aerosol Partitioning Model. *Environ. Sci. Technol.* **1999**, *33*, 1430−1438.
(6) Zhang, Y.; Sanchez, M. S.; Douet, C.; Wang, Y.; Bateman, A. P.; Gong, Z.; Kuwata, M.; Renbaum-Wolff, L.; Sato, B. B.; Liu, P. F.; Bertram, A. K.; Geiger, F. M.; Martin, S. T. Changing shapes and implied viscosities of suspended submicron particles. *Atmos. Chem. Phys.* **2015**, *15*, 7819−7829.
(7) Renbaum-Wolff, L.; Grayson, J. W.; Bateman, A. P.; Kuwata, M.; Sellier, M.; Murray, B. J.; Shilling, J. E.; Martin, S. T.; Bertram, A. K. Viscosity of α-pinene secondary organic material and implications for particle growth and reactivity. *Proc. Natl. Acad. Sci. U. S. A.* **2013**, *110*, 8014−8019.
(8) Rothfuss, N. E.; Petters, M. D. Coalescence-based assessment of aerosol phase state using dimers prepared through a dual-differential mobility analyzer technique. *Aerosol Sci. Technol.* **2016**, *50*, 1294−1305.
(9) Shrestha, M.; Zhang, Y.; Upshur, M. A.; Liu, P.; Blair, S. L.; Wang, H.-f.; Nizkorodov, S. A.; Thomson, R. J.; Martin, S. T.; Geiger, F. M. On surface order and disorder of α-pinene-derived secondary organic material. *J. Phys. Chem. A* **2014**, *119*, 4609−4617.
(10) Liu, P.; Li, Y. J.; Wang, Y.; Bateman, A. P.; Zhang, Y.; Gong, Z.; Bertram, A. K.; Martin, S. T. Highly Viscous States Affect the Browning of Atmospheric Organic Particulate Matter. *ACS Cent. Sci.* **2018**, 207.
(11) Slade, J. H.; Ault, A. P.; Bui, A. T.; Ditto, J. C.; Lei, Z.; Bondy, A. L.; Olson, N. E.; Cook, R. D.; Desrochers, S. J.; Harvey, R. M.; Erickson, M. H.; Wallace, H. W.; Alvarez, S. L.; Flynn, J. H.; Boor, B. E.; Petrucci, G. A.; Gentner, D. R.; Griffin, R. J.; Shepson, P. B. Bouncier Particles at Night: Biogenic Secondary Organic Aerosol Chemistry and Sulfate Drive Diel Variations in the Aerosol Phase in a Mixed Forest. *Environ. Sci. Technol.* **2019**, *53*, 4977−4987.
(12) Pajunoja, A.; Hu, W.; Leong, Y. J.; Taylor, N. F.; Miettinen, P.; Palm, B. B.; Mikkonen, S.; Collins, D. R.; Jimenez, J. L.; Virtanen, A. Phase state of ambient aerosol linked with water uptake and chemical aging in the southeastern US. *Atmos. Chem. Phys.* **2016**, *16*, 11163−11176.
(13) Bateman, A. P.; Gong, Z.; Liu, P.; Sato, B.; Cirino, G.; Zhang, Y.; Artaxo, P.; Bertram, A. K.; Manzi, A. O.; Rizzo, L. V.; Souza, R. A. F.; Zaveri, R. A.; Martin, S. T. Sub-micrometre particulate matter is primarily in liquid form over Amazon rainforest. *Nat. Geosci.* **2015**, *9*, 34.
(14) Virtanen, A.; Joutsensaari, J.; Koop, T.; Kannosto, J.; Yli-Pirilä, P.; Leskinen, J.; Mäkelä, J. M.; Holopainen, J. K.; Pöschl, U.; Kulmala, M.; Worsnop, D. R.; Laaksonen, A. An amorphous solid state of biogenic secondary organic aerosol particles. *Nature* **2010**, *467*, 824−827.
(15) Saukko, E.; Lambe, A. T.; Massoli, P.; Koop, T.; Wright, J. P.; Croasdale, D. R.; Pedernera, D. A.; Onasch, T. B.; Laaksonen, A.; Davidovits, P.; Worsnop, D. R.; Virtanen, A. Humidity-dependent phase state of SOA particles from biogenic and anthropogenic precursors. *Atmos. Chem. Phys.* **2012**, *12*, 7517−7529.
(16) Valorso, R.; Aumont, B.; Camredon, M.; Raventos-Duran, T.; Mouchel-Vallon, C.; Ng, N. L.; Seinfeld, J. H.; Lee-Taylor, J.; Madronich, S. Explicit modelling of SOA formation from α-pinene photooxidation: sensitivity to vapour pressure estimation. *Atmos. Chem. Phys.* **2011**, *11*, 6895−6910.
(17) Liu, Y.; Kuwata, M.; Strick, B. F.; Geiger, F. M.; Thomson, R. J.; McKinney, K. A.; Martin, S. T. Uptake of Epoxydiol Isomers Accounts for Half of the Particle-Phase Material Produced from Isoprene Photooxidation via the HO_2 Pathway. *Environ. Sci. Technol.* **2014**, *49*, 250−258.
(18) Surratt, J. D.; Chan, A. W. H.; Eddingsaas, N. C.; Chan, M.; Loza, C. L.; Kwan, A. J.; Hersey, S. P.; Flagan, R. C.; Wennberg, P. O.; Seinfeld, J. H. Reactive intermediates revealed in secondary organic aerosol formation from isoprene. *Proc. Natl. Acad. Sci. U. S. A.* **2010**, *107*, 6640−5.
(19) Zhang, H.; Surratt, J. D.; Lin, Y. H.; Bapat, J.; Kamens, R. M. Effect of relative humidity on SOA formation from isoprene/NO photooxidation: enhancement of 2-methylglyceric acid and its corresponding oligoesters under dry conditions. *Atmos. Chem. Phys.* **2011**, *11*, 6411−6424.
(20) Lin, Y.-H.; Zhang, Z.; Docherty, K. S.; Zhang, H.; Budisulistiorini, S. H.; Rubitschun, C. L.; Shaw, S. L.; Knipping, E. M.; Edgerton, E. S.; Kleindienst, T. E.; Gold, A.; Surratt, J. D. Isoprene epoxydiols as precursors to secondary organic aerosol formation: acid-catalyzed reactive uptake studies with authentic compounds. *Environ. Sci. Technol.* **2012**, *46*, 250−8.
(21) Gaston, C. J.; Riedel, T. P.; Zhang, Z.; Gold, A.; Surratt, J. D.; Thornton, J. A. Reactive Uptake of an Isoprene-Derived Epoxydiol to Submicron Aerosol Particles. *Environ. Sci. Technol.* **2014**, *48*, 11178−11186.
(22) Zhang, Y.; Chen, Y.; Lambe, A. T.; Olson, N. E.; Lei, Z.; Craig, R. L.; Zhang, Z.; Gold, A.; Onasch, T. B.; Jayne, J. T.; Worsnop, D. R.; Gaston, C. J.; Thornton, J. A.; Vizuete, W.; Ault, A. P.; Surratt, J. D. Effect of the Aerosol-Phase State on Secondary Organic Aerosol Formation from the Reactive Uptake of Isoprene-Derived Epoxydiols (IEPOX). *Environ. Sci. Technol. Lett.* **2018**, *5*, 167−174.
(23) Cui, T.; Zeng, Z.; dos Santos, E. O.; Zhang, Z.; Chen, Y.; Zhang, Y.; Rose, C. A.; Budisulistiorini, S. H.; Collins, L. B.; Bodnar, W. M.; de Souza, R. A. F.; Martin, S. T.; Machado, C. M. D.; Turpin, B. J.; Gold, A.; Ault, A. P.; Surratt, J. D. Development of a hydrophilic interaction liquid chromatography (HILIC) method for the chemical characterization of water-soluble isoprene epoxydiol (IEPOX)-derived secondary organic aerosol. *Environ. Sci.: Processes Impacts* **2018**, *20*, 1524−1536.
(24) Zhang, Y.; Liu, P.; Gong, Z.; Geiger, F. M.; Martin, S. T. Production and Measurement of Organic Particulate Matter in a Flow Tube Reactor. *J. Visualized Exp.* **2018**, *142*, No. e55684.
(25) Zhang, Y.; Gong, Z.; Sa, S. d.; Bateman, A. P.; Liu, Y.; Li, Y.; Geiger, F. M.; Martin, S. T. Production and Measurement of Organic Particulate Matter in the Harvard Environmental Chamber. *J. Visualized Exp.* **2018**, No. e55685.
(26) Knopf, D. A.; Alpert, P. A.; Wang, B. The Role of Organic Aerosol in Atmospheric Ice Nucleation: A Review. *ACS Earth Space Chem.* **2018**, *2*, 168−202.
(27) Koop, T.; Bookhold, J.; Shiraiwa, M.; Pöschl, U. Glass transition and phase state of organic compounds: dependency on molecular properties and implications for secondary organic aerosols in the atmosphere. *Phys. Chem. Chem. Phys.* **2011**, *13*, 19238−19255.

DOI: 10.1021/acs.est.9b03317
Environ. Sci. Technol. XXXX, XXX, XXX−XXX

(28) Keys, A. S.; Garrahan, J. P.; Chandler, D. Calorimetric glass transition explained by hierarchical dynamic facilitation. *Proc. Natl. Acad. Sci. U. S. A.* **2013**, *110*, 4482−4487.
(29) Reid, J. P.; Bertram, A. K.; Topping, D. O.; Laskin, A.; Martin, S. T.; Petters, M. D.; Pope, F. D.; Rovelli, G. The viscosity of atmospherically relevant organic particles. *Nat. Commun.* **2018**, *9*, 956.
(30) Zobrist, B.; Soonsin, V.; Luo, B. P.; Krieger, U. K.; Marcolli, C.; Peter, T.; Koop, T. Ultra-slow water diffusion in aqueous sucrose glasses. *Phys. Chem. Chem. Phys.* **2011**, *13*, 3514−3526.
(31) Shiraiwa, M.; Zuend, A.; Bertram, A. K.; Seinfeld, J. H. Gas-particle partitioning of atmospheric aerosols: interplay of physical state, non-ideal mixing and morphology. *Phys. Chem. Chem. Phys.* **2013**, *15*, 11441−11453.
(32) Shiraiwa, M.; Berkemeier, T.; Schilling-Fahnestock, K. A.; Seinfeld, J. H.; Pöschl, U. Molecular corridors and kinetic regimes in the multiphase chemical evolution of secondary organic aerosol. *Atmos. Chem. Phys.* **2014**, *14*, 8323−8341.
(33) Price, H. C.; Mattsson, J.; Zhang, Y.; Bertram, A. K.; Davies, J. F.; Grayson, J. W.; Martin, S. T.; O'Sullivan, D.; Reid, J. P.; Rickards, A. M. J.; Murray, B. J. Water diffusion in atmospherically relevant α-pinene secondary organic material. *Chem. Sci.* **2015**, *6*, 4876−4883.
(34) Baustian, K. J.; Wise, M. E.; Jensen, E. J.; Schill, G. P.; Freedman, M. A.; Tolbert, M. A. State transformations and ice nucleation in amorphous (semi-)solid organic aerosol. *Atmos. Chem. Phys.* **2013**, *13*, 5615−5628.
(35) Schill, G. P.; Tolbert, M. A. Heterogeneous ice nucleation on phase-separated organic-sulfate particles: effect of liquid vs. glassy coatings. *Atmos. Chem. Phys.* **2013**, *13*, 4681−4695.
(36) Zobrist, B.; Marcolli, C.; Pedernera, D. A.; Koop, T. Do atmospheric aerosols form glasses? *Atmos. Chem. Phys.* **2008**, *8*, 5221−5244.
(37) Dette, H. P.; Koop, T. Glass Formation Processes in Mixed Inorganic/Organic Aerosol Particles. *J. Phys. Chem. A* **2015**, *119*, 4552−4561.
(38) Dette, H. P.; Qi, M.; Schröder, D. C.; Godt, A.; Koop, T. Glass-Forming Properties of 3-Methylbutane-1,2,3-tricarboxylic Acid and Its Mixtures with Water and Pinonic Acid. *J. Phys. Chem. A* **2014**, *118*, 7024−7033.
(39) Lienhard, D. M.; Huisman, A. J.; Krieger, U. K.; Rudich, Y.; Marcolli, C.; Luo, B. P.; Bones, D. L.; Reid, J. P.; Lambe, A. T.; Canagaratna, M. R.; Davidovits, P.; Onasch, T. B.; Worsnop, D. R.; Steimer, S. S.; Koop, T.; Peter, T. Viscous organic aerosol particles in the upper troposphere: diffusivity-controlled water uptake and ice nucleation? *Atmos. Chem. Phys.* **2015**, *15*, 13599−13613.
(40) Berkemeier, T.; Shiraiwa, M.; Pöschl, U.; Koop, T. Competition between water uptake and ice nucleation by glassy organic aerosol particles. *Atmos. Chem. Phys.* **2014**, *14*, 12513−12531.
(41) Debenedetti, P. G.; Stillinger, F. H. Supercooled liquids and the glass transition. *Nature* **2001**, *410*, 259−267.
(42) Elmatad, Y. S.; Chandler, D.; Garrahan, J. P. Corresponding States of Structural Glass Formers. II. *J. Phys. Chem. B* **2010**, *114*, 17113−17119.
(43) Elmatad, Y. S.; Chandler, D.; Garrahan, J. P. Corresponding States of Structural Glass Formers. *J. Phys. Chem. B.* **2009**, *113*, 5563−5567.
(44) Zhang, Y.; Katira, S.; Lee, A.; Lambe, A. T.; Onasch, T. B.; Xu, W.; Brooks, W. A.; Canagaratna, M. R.; Freedman, A.; Jayne, J. T.; Worsnop, D. R.; Davidovits, P.; Chandler, D.; Kolb, C. E. Kinetically controlled glass transition measurement of organic aerosol thin films using broadband dielectric spectroscopy. *Atmos. Meas. Tech.* **2018**, *11*, 3479−3490.
(45) Riedel, T. P.; Lin, Y. H.; Zhang, Z.; Chu, K.; Thornton, J. A.; Vizuete, W.; Gold, A.; Surratt, J. D. Constraining condensed-phase formation kinetics of secondary organic aerosol components from isoprene epoxydiols. *Atmos. Chem. Phys.* **2016**, *16*, 1245−1254.
(46) Zhang, Z.; Lin, Y. H.; Zhang, H.; Surratt, J. D.; Ball, L. M.; Gold, A. Technical Note: Synthesis of isoprene atmospheric oxidation products: isomeric epoxydiols and the rearrangement products *cis*- and *trans*-3-methyl-3,4-dihydroxytetrahydrofuran. *Atmos. Chem. Phys.* **2012**, *12*, 8529−8535.
(47) Lin, Y.-H.; Zhang, H.; Pye, H. O. T.; Zhang, Z.; Marth, W. J.; Park, S.; Arashiro, M.; Cui, T.; Budisulistiorini, S. H.; Sexton, K. G.; Vizuete, W.; Xie, Y.; Luecken, D. J.; Piletic, I. R.; Edney, E. O.; Bartolotti, L. J.; Gold, A.; Surratt, J. D. Epoxide as a precursor to secondary organic aerosol formation from isoprene photooxidation in the presence of nitrogen oxides. *Proc. Natl. Acad. Sci. U. S. A.* **2013**, *110*, 6718−6723.
(48) Riva, M.; Bell, D. M.; Hansen, A.-M. K.; Drozd, G. T.; Zhang, Z.; Gold, A.; Imre, D.; Surratt, J. D.; Glasius, M.; Zelenyuk, A. Effect of Organic Coatings, Humidity and Aerosol Acidity on Multiphase Chemistry of Isoprene Epoxydiols. *Environ. Sci. Technol.* **2016**, *50*, 5580−5588.
(49) Liu, P.; Zhang, Y.; Martin, S. T. Complex Refractive Indices of Thin Films of Secondary Organic Materials by Spectroscopic Ellipsometry from 220 to 1200 nm. *Environ. Sci. Technol.* **2013**, *47*, 13594−13601.
(50) Chen, Z.; Sepúlveda, A.; Ediger, M. D.; Richert, R. Dielectric spectroscopy of thin films by dual-channel impedance measurements on differential interdigitated electrode arrays. *Eur. Phys. J. B* **2012**, *85*, 268.
(51) Böhmer, R.; Ngai, K. L.; Angell, C. A.; Plazek, D. J. Nonexponential relaxations in strong and fragile glass formers. *J. Chem. Phys.* **1993**, *99*, 4201−4209.
(52) Keys, A. S.; Hedges, L. O.; Garrahan, J. P.; Glotzer, S. C.; Chandler, D. Excitations Are Localized and Relaxation Is Hierarchical in Glass-Forming Liquids. *Phys. Rev. X* **2011**, *1*, No. 021013.
(53) Chandler, D.; Garrahan, J. P. Dynamics on the Way to Forming Glass: Bubbles in Space-Time. *Annu. Rev. Phys. Chem.* **2010**, *61*, 191−217.
(54) Hudson, A.; Mandadapu, K. K. On the nature of the glass transition in atomistic models of glass formers. 2018, 1−13. http://arxiv.org/abs/1804.03769.
(55) Lessmeier, J.; Dette, H. P.; Godt, A.; Koop, T. Physical state of 2-methylbutane-1,2,3,4-tetraol in pure and internally mixed aerosols. *Atmos. Chem. Phys.* **2018**, *18*, 15841−15857.
(56) Jensen, M. H.; Gainaru, C.; Alba-Simionesco, C.; Hecksher, T.; Niss, K. Slow rheological mode in glycerol and glycerol−water mixtures. *Phys. Chem. Chem. Phys.* **2018**, *20*, 1716−1723.
(57) Murray, B. J.; Wilson, T. W.; Dobbie, S.; Cui, Z.; Al-Jumur, S. M. R. K.; Möhler, O.; Schnaiter, M.; Wagner, R.; Benz, S.; Niemand, M.; Saathoff, H.; Ebert, V.; Wagner, S.; Kärcher, B. Heterogeneous nucleation of ice particles on glassy aerosols under cirrus conditions. *Nat. Geosci.* **2010**, *3*, 233−237.
(58) Wolf, M. J.; Coe, A.; Dove, L. A.; Zawadowicz, M. A.; Dooley, K.; Biller, S. J.; Zhang, Y.; Chisholm, S. W.; Cziczo, D. J. Investigating the Heterogeneous Ice Nucleation of Sea Spray Aerosols Using Prochlorococcus as a Model Source of Marine Organic Matter. *Environ. Sci. Technol.* **2019**, *53*, 1139−1149.
(59) Thomas, L. H.; Meatyard, R.; Smith, H.; Davies, G. H. Viscosity behavior of associated liquids at lower temperatures and vapor pressures. *J. Chem. Eng. Data* **1979**, *24*, 161−164.
(60) Mitra, S. S. Relation between Vapor Pressure and Viscosity of Liquids. *J. Chem. Phys.* **1954**, *22*, 349−350.
(61) Lohmann, J.; Joh, R.; Gmehling, J. Estimation of Enthalpies of Fusion, Melting Temperatures, Enthalpies of Transition, and Transition Temperatures of Pure Compounds from Experimental Binary Solid−Liquid Equilibrium Data of Eutectic Systems. *J. Chem. Eng. Data* **1997**, *42*, 1176−1180.
(62) Trouton, F. IV. On molecular latent heat. *Lond. Edinb. Dubl. Phil. Mag.* **1884**, *18*, 54−57.
(63) Wang, L.-M.; Richert, R. Glass Transition Dynamics and Boiling Temperatures of Molecular Liquids and Their Isomers. *J. Phys. Chem. B* **2007**, *111*, 3201−3207.
(64) Shiraiwa, M.; Li, Y.; Tsimpidi, A. P.; Karydis, V. A.; Berkemeier, T.; Pandis, S. N.; Lelieveld, J.; Koop, T.; Pöschl, U. Global distribution of particle phase state in atmospheric secondary organic aerosols. *Nat. Commun.* **2017**, *8*, 15002.

DOI: 10.1021/acs.est.9b03317
Environ. Sci. Technol. XXXX, XXX, XXX−XXX

(65) Cammenga, H. K.; Schulze, F. W.; Theuerl, W. Vapor pressure and evaporation coefficient of glycerol. *J. Chem. Eng. Data* **1977**, *22*, 131−134.
(66) Cai, C.; Stewart, D. J.; Reid, J. P.; Zhang, Y.-H.; Ohm, P.; Dutcher, C. S.; Clegg, S. L. Organic Component Vapor Pressures and Hygroscopicities of Aqueous Aerosol Measured by Optical Tweezers. *J. Phys. Chem. A* **2015**, *119*, 704−718.
(67) Ray, A. K.; Davis, E. J.; Ravindran, P. Determination of ultra-low vapor pressures by submicron droplet evaporation. *J. Chem. Phys.* **1979**, *71*, 582−587.
(68) Huisman, A. J.; Krieger, U. K.; Zuend, A.; Marcolli, C.; Peter, T. Vapor pressures of substituted polycarboxylic acids are much lower than previously reported. *Atmos. Chem. Phys.* **2013**, *13*, 6647−6662.
(69) King, R. B. *Encyclopedia of Inorganic Chemistry*; John Wiley & Sons Ltd: 2006.
(70) Krzyzaniak, J. F.; Myrdal, P. B.; Simamora, P.; Yalkowsky, S. H. Boiling Point and Melting Point Prediction for Aliphatic, Non-Hydrogen-Bonding Compounds. *Ind. Eng. Chem. Res.* **1995**, *34*, 2530−2535.
(71) Pankow, J. F. An absorption model of the gas/aerosol partitioning involved in the formation of secondary organic aerosol. *Atmos. Environ.* **1994**, *28*, 189−193.
(72) Zuend, A.; Seinfeld, J. H. Modeling the gas-particle partitioning of secondary organic aerosol: the importance of liquid-liquid phase separation. *Atmos. Chem. Phys.* **2012**, *12* (9), 3857−3882.
(73) Beirnes, K. J.; Burns, C. M. Thermal analysis of the glass transition of plasticized poly(vinyl chloride). *J. Appl. Polym. Sci.* **1986**, *31*, 2561−2567.
(74) Shinyashiki, N.; Shinohara, M.; Iwata, Y.; Goto, T.; Oyama, M.; Suzuki, S.; Yamamoto, W.; Yagihara, S.; Inoue, T.; Oyaizu, S.; Yamamoto, S.; Ngai, K. L.; Capaccioli, S. The Glass Transition and Dielectric Secondary Relaxation of Fructose−Water Mixtures. *J. Phys. Chem. B* **2008**, *112*, 15470−15477.
(75) Dorfmüller, T.; Dux, H.; Fytas, G.; Mersch, W. A light scattering study of the molecular motion in hexanetriol 1,2,6. *J. Chem. Phys.* **1979**, *71*, 366−375.
(76) DeRieux, W. S. W.; Li, Y.; Lin, P.; Laskin, J.; Laskin, A.; Bertram, A. K.; Nizkorodov, S. A.; Shiraiwa, M. Predicting the glass transition temperature and viscosity of secondary organic material using molecular composition. *Atmos. Chem. Phys.* **2018**, *18*, 6331−6351.
(77) Simamora, P.; Yalkowsky, S. H. Quantitative Structure Property Relationship in the Prediction of Melting Point and Boiling Point of Rigid Non-Hydrogen Bonding Organic Molecules. *SAR QSAR Environ. Res.* **1993**, *1*, 293−300.
(78) Wang, L. M.; Tian, Y.; Liu, R.; Richert, R. Calorimetric versus kinetic glass transitions in viscous monohydroxy alcohols. *J. Chem. Phys.* **2008**, *128*, 084503.
(79) Kidd, C.; Perraud, V.; Wingen, L. M.; Finlayson-Pitts, B. J. Integrating phase and composition of secondary organic aerosol from the ozonolysis of α-pinene. *Proc. Natl. Acad. Sci. U. S. A.* **2014**, *111*, 7552−7557.
(80) Moynihan, C. T.; Easteal, A. J.; Wilder, J.; Tucker, J. Dependence of the glass transition temperature on heating and cooling rate. *J. Chem. Phys.* **1974**, *78*, 2673−2677.
(81) Claflin, M. S.; Krechmer, J. E.; Hu, W.; Jimenez, J. L.; Ziemann, P. J. Functional Group Composition of Secondary Organic Aerosol Formed from Ozonolysis of α-Pinene Under High VOC and Autoxidation Conditions. *ACS Earth Space Chem.* **2018**, *2*, 1196−1210.
(82) Sareen, N.; Carlton, A. G.; Surratt, J. D.; Gold, A.; Lee, B.; Lopez-Hilfiker, F. D.; Mohr, C.; Thornton, J. A.; Zhang, Z.; Lim, Y. B.; Turpin, B. J. Identifying precursors and aqueous organic aerosol formation pathways during the SOAS campaign. *Atmos. Chem. Phys.* **2016**, *16*, 14409−14420.
(83) Martin, S. T.; Artaxo, P.; Machado, L.; Manzi, A. O.; Souza, R. A. F.; Schumacher, C.; Wang, J.; Biscaro, T.; Brito, J.; Calheiros, A.; Jardine, K.; Medeiros, A.; Portela, B.; De Sá, S. S.; Adachi, K.; Aiken, A. C.; Albrecht, R.; Alexander, L.; Andreae, M. O.; Barbosa, H. M. J.; Buseck, P. R.; Chand, D.; Comstock, J. M.; Day, D. A.; Dubey, M.; Fan, J.; Fast, J.; Fisch, G.; Fortner, E.; Giangrande, S.; Gilles, M.; Goldstein, A. H.; Guenther, A.; Hubbe, J.; Jensen, M.; Jimenez, J. L.; Keutstsch, F. N.; Kim, S.; Kuang, C.; Laskin, A.; McKinney, K.; Mei, F.; Miller, M.; Nascimento, R.; Pauliquevis, T.; Pekour, M.; Peres, J.; Petäjä, T.; Pöhlker, C.; Pöschl, U.; Rizzo, L.; Schmid, B.; Shilling, J. E.; Silva Dias, M. A.; Smith, J. N.; Tomlinson, J. M.; Tóta, J.; Wendisch, M. The green ocean amazon experiment (GOAMAZON2014/5) observes pollution affecting gases, aerosols, clouds, and rainfall over the rain forest. *Bull. Am. Meteorol. Soc.* **2017**, *98*, 981−997.
(84) Brostow, W.; Chiu, R.; Kalogeras, I. M.; Vassilikou-Dova, A. Prediction of glass transition temperatures: Binary blends and copolymers. *Mater. Lett.* **2008**, *62*, 3152−3155.
(85) Ahmed, J. *Glass Transition and Phase Transitions in Food and Biological Materials*; Wiley-Blackwell: 2017.
(86) Bock, D.; Körber, T.; Mohamed, F.; Pötzschner, B.; Rössler, E. A., Dynamic Heterogeneities in Binary Glass-Forming Systems. In *The Scaling of Relaxation Processes*; Kremer, F.; Loidl, A., Eds. Springer International Publishing: Cham, 2018; pp 173−201.
(87) Pinal, R. Entropy of Mixing and the Glass Transition of Amorphous Mixtures. *Entropy* **2008**, *10*, 207−223.
(88) Margenau, H. Van der waals forces. *Rev. Mod. Phys.* **1939**, *11*, 1−35.
(89) Li, Y.; Shiraiwa, M. Timescales of secondary organic aerosols to reach equilibrium at various temperatures and relative humidities. *Atmos. Chem. Phys.* **2019**, *19*, 5959−5971.
(90) Riva, M.; Chen, Y.; Zhang, Y.; Lei, Z.; Olson, N.; Boyer, H. C.; Narayan, S.; Yee, L. D.; Green, H.; Cui, T.; Zhang, Z.; Baumann, K. D.; Fort, M.; Edgerton, E. S.; Budisulistiorini, S.; Rose, C. A.; Ribeiro, I.; e Oliveira, R. L.; Santos, E.; Szopa, S.; Machado, C.; Zhao, Y.; Alves, E.; de Sa, S.; Hu, W.; Knipping, E.; Shaw, S.; Duvoisin Junior, S.; Souza, R. A. F. d.; Palm, B. B.; Jimenez, J. L.; Glasius, M.; Goldstein, A. H.; Pye, H. O. T.; Gold, A.; Turpin, B. J.; Vizuete, W.; Martin, S. T.; Thornton, J.; Dutcher, C. S.; Ault, A. P.; Surratt, J. D. Increasing Isoprene Epoxydiol-to-Inorganic Sulfate Aerosol Ratio Results in Extensive Conversion of Inorganic Sulfate to Organosulfur Forms: Implications for Aerosol Physicochemical Properties. *Environ. Sci. Technol.* **2019**, 8682.
(91) Rivera-Rios, J. C.; Nguyen, T. B.; Crounse, J. D.; Jud, W.; St. Clair, J. M.; Mikoviny, T.; Gilman, J. B.; Lerner, B. M.; Kaiser, J. B.; Gouw, J.; Wisthaler, A.; Hansel, A.; Wennberg, P. O.; Seinfeld, J. H.; Keutsch, F. N. Conversion of hydroperoxides to carbonyls in field and laboratory instrumentation: Observational bias in diagnosing pristine versus anthropogenically controlled atmospheric chemistry. *Geophys. Res. Lett.* **2015**, *41*, 8645−8651.
(92) Compernolle, S.; Ceulemans, K.; Müller, J. F. EVAPORATION: a new vapour pressure estimation methodfor organic molecules including non-additivity and intramolecular interactions. *Atmos. Chem. Phys.* **2011**, *11*, 9431−9450.
(93) Rothfuss, N. E.; Petters, M. D. Influence of Functional Groups on the Viscosity of Organic Aerosol. *Environ. Sci. Technol.* **2016**, *51*, 271−279.
(94) US-EPA. *Estimation Program Interface (EPI) Suite Ver. 4.1* [Online], 2010.
(95) Kostenidou, E.; Karnezi, E.; Kolodziejczyk, A.; Szmigielski, R.; Pandis, S. N. Physical and Chemical Properties of 3-Methyl-1,2,3-butanetricarboxylic Acid (MBTCA) Aerosol. *Environ. Sci. Technol.* **2018**, *52*, 1150−1155.
(96) Budisulistiorini, S. H.; Nenes, A.; Carlton, A. G.; Surratt, J. D.; McNeill, V. F.; Pye, H. O. T. Simulating Aqueous-Phase Isoprene-Epoxydiol (IEPOX) Secondary Organic Aerosol Production During the 2013 Southern Oxidant and Aerosol Study (SOAS). *Environ. Sci. Technol.* **2017**, *51*, 5026−5034.
(97) Li, Y.; Pöschl, U.; Shiraiwa, M. Molecular corridors and parameterizations of volatility in the chemical evolution of organic aerosols. *Atmos. Chem. Phys.* **2016**, *16*, 3327−3344.
(98) Lu, Q.; Zografi, G. Properties of citric acid at the glass transition. *J. Pharm. Sci.* **1997**, *86*, 1374−8.

DOI: 10.1021/acs.est.9b03317
Environ. Sci. Technol. XXXX, XXX, XXX−XXX

(99) Lienhard, D. M.; Zobrist, B.; Zuend, A.; Krieger, U. K.; Peter, T. Experimental evidence for excess entropy discontinuities in glass-forming solutions. *J. Chem. Phys.* **2012**, *136*, 074515.
(100) Nakanishi, M.; Nozaki, R. Dynamics and structure of hydrogen-bonding glass formers: Comparison between hexanetriol and sugar alcohols based on dielectric relaxation. *Phys. Rev. E* **2010**, *81*, 041501.
(101) Bilde, M.; Pandis, S. N. Evaporation Rates and Vapor Pressures of Individual Aerosol Species Formed in the Atmospheric Oxidation of α- and β-Pinene. *Environ. Sci. Technol.* **2001**, *35*, 3344−3349.
(102) Dufour, J.; Jorat, L.; Bondeau, A.; Siblini, A.; Noyel, G. Shear viscosity and dielectric relaxanon time of dibutyl phthalate down to glass transition temperature. *J. Mol. Liq.* **1994**, *62*, 75−82.
(103) Gobble, C.; Chickos, J.; Verevkin, S. P. Vapor Pressures and Vaporization Enthalpies of a Series of Dialkyl Phthalates by Correlation Gas Chromatography. *J. Chem. Eng. Data* **2014**, *59*, 1353−1365.
(104) Pankow, J. F.; Asher, W. E. SIMPOL.1: a simple group contribution method for predicting vapor pressures and enthalpies of vaporization of multifunctional organic compounds. *Atmos. Chem. Phys.* **2008**, *8*, 2773−2796.
(105) Amann-Winkel, K.; Gainaru, C.; Handle, P. H.; Seidl, M.; Nelson, H.; Böhmer, R.; Loerting, T. Water's second glass transition. *Proc. Natl. Acad. Sci. U. S. A.* **2013**, *110*, 17720−17725.

NOTE ADDED AFTER ASAP PUBLICATION

This article published October 9, 2019 with errors in equation 3. The corrected article published October 11, 2019.

DOI: 10.1021/acs.est.9b03317
Environ. Sci. Technol. XXXX, XXX, XXX−XXX